An Optical Nanocavity Incorporating a Fluorescent Organic Dye Having a High Quality Factor

Ali M. Adawi,[†,*] Mohamed M. Murshidy,[†,§] Paul W. Fry,[‡] and David G. Lidzey[†,*]

[†]Department of Physics and Astronomy, The University of Sheffield, Hicks Building, Hounsfield Road, Sheffield S3 7RH, United Kingdom, [‡]Nanoscience and Technology Centre, University of Sheffield, North Campus, Broad Lane, Sheffield, S3 7HQ, United Kingdom., and [§]Department of Physics, Faculty of Science, Helwan University, Helwan, Egypt

ABSTRACT We have fabricated an *L*3 optical nanocavity operating at visible wavelengths that is coated with a thin-film of a fluorescent molecular-dye. The cavity was directly fabricated into a pre-etched, free-standing silicon-nitride (SiN) membrane and had a quality factor of $Q = 2650$. This relatively high *Q*-factor approaches the theoretical limit that can be expected from an *L*3 nanocavity using silicon nitride as a dielectric material and is achieved as a result of the solvent-free cavity-fabrication protocol that we have developed. We show that the fluorescence from a red-emitting fluorescent dye coated onto the cavity surface undergoes strong emission intensity enhancement at a series of discrete wavelengths corresponding to the cavity modes. Three dimensional finite difference time domain (FDTD) calculations are used to predict the mode structure of the cavities with excellent agreement demonstrated between theory and experiment.

KEYWORDS: optical nanocavity · photonic crystal · organic-semiconductor · fluorescent molecular-dye · finite difference time domain calculations

In recent years organic-semiconductors have attracted much attention as materials for the study of fundamental physics[1−5] and for their potential technological applications in molecular optoelectronics and photonics.[6−14] In applications involving the absorption or emission of radiation, it is often necessary to confine the electromagnetic field surrounding an emitting dipole—an approach that is used to generate optical feedback in organic-based lasers.[8−14] Indeed, the strength of the optical-confinement generated by a structure can be quantified using the ratio *Q*/*V*. Here, *Q* is the quality factor of the optical resonator and is a measure of the confinement lifetime of photons by the cavity, and *V* is the mode volume of the resonator and describes the strength of the optical field peak within the cavity ($V \propto 1/\sqrt{E_p}$). Structures with a large *Q*/*V* ratio are a prerequisite for the generation of a significant enhancement in the spontaneous emission rate *via* the Fermi Golden Rule.[15,16] High *Q*-factors are also advantageous for creating effective optical feedback and thus the generation of low threshold laser structures.[17,18]

Until now, most work creating optical cavities containing organic materials have utilized either simple one-dimensional (1-D) microcavities[9,14,19−21] or two-dimensional distributed feedback (DFB) resonators.[10,11] Here, typical *Q*-factors of ~1000 have been demonstrated in 1-D optical microcavities containing thin organic films.[14,20,21] Such structures however lack the three-dimensional confinement required to achieve a small mode volume and thereby generate a large modification in optical transition rates. Microcavity micropillars[13,22,23] can provide three-dimensional optical confinement; however, their experimental *Q*/*V* ratio is limited to around 500 μm^{-3}.[22] Dye-doped polymer microspheres can support optical modes with a *Q*-factor between 1000 and 10000;[8] however, the mode volume of such microspheres is relatively large[24]—a condition that limits typical *Q*/*V* ratios to around 100 μm^{-3}.

Recently, two-dimensional photonic crystal (2DPC) nanocavities have emerged as attractive structures in which to achieve very high *Q*/*V* ratios. Such structures are formed by deliberately introducing a physical defect into a two-dimensional photonic crystal.[25] The main advantage of 2DPCs over other types of optical resonators are their very small mode volume (of the order of $(\lambda/n)^3 \sim 0.035$ to 0.085 μm^3)[26,27] combined with *Q*-factors ranging between a few thousand for materials of refractive index $n \sim 2$ (e.g., silicon nitride (SiN) or diamond)[28] to over a million for materials of refractive index $n \sim 3.4$ (e.g., silicon or GaAs).[27,29]

Several attempts have been made to create 2DPC nanocavities based on a

*Address correspondence to a.adawi@sheffield.ac.uk, d.g.lidzey@sheffield.ac.uk.

Received for review January 25, 2010 and accepted May 19, 2010.

Published online May 25, 2010. 10.1021/nn1001479

dielectric material that has been coated with an organic thin film. As most organic materials absorb or emit light at visible wavelengths, it is necessary to use high electronic band gap ($E_g > 3.1$ eV) dielectric materials to fabricate the cavity to reduce optical loss by absorption in the dielectric. Such high electronic band gap materials however have a relatively low refractive index ($n < 2.4$); an effect which reduces the effective ability of the cavity to confine photons and thus limits the *Q*-factor of the resultant structure. For example Kitamura *et al.*[30] fabricated one-missing-air-hole 2DPC nanocavities based on Alq_3/SiO_2, having a *Q*-factor of 1000. This value was however further limited because of the lack of refractive index continuity in the vertical direction of the photonic crystal slab. Barth *et al.*[31] have also reported the fabrication of 2DPC nanocavities consisting of three missing aligned air holes with some modifications to the size and position of the air holes surrounding the cavity (known as a modified *L*3 cavity) based on SiN coated with a thin-film of the molecular dye Nile Red. Here the nanocavity structures reported had a *Q*-factor of 1500. Recently, we have reported the fabrication of a regular *L*3 nanocavity defined in a free-standing SiN membrane having a *Q*-factor of 1300.[32] Despite this progress, there is still significant interest in developing organic-based nanocavities with much higher *Q*-factors, as such structures could form the basis of a low threshold nanolaser or a single-photon device. Such increases in *Q*-factor can in principle be realized by improved optical design and by reducing the density of physical defects in the cavity structure. Such defects are known to act as scattering centers and thereby introduce optical loss. In addition to this, cavity *Q*-factor can be increased by minimizing the vertical taper of the air holes surrounding the nanocavity. Any such taper will generate a vertical asymmetry in the structure and will lead to a coupling between TE and TM-like modes, thus resulting in optical loss.[33]

In this paper we describe the fabrication and characterization of the optical properties of a nanocavity having the highest *Q*-factor yet reported for an organic/SiN based system ($Q = 2650$). The structures fabricated utilize SiN to create a 2D resonator structure and are coated with a thin film of an emissive organic chromophore. As we describe below, we achieve high *Q*-factors by directly patterning a free-standing silicon nitride membrane using only dry-etch-based processes—a technique that permits us to create photonic crystal holes having a low taper angle (2.5°). Such high *Q*-factor cavities containing organic materials will be of significant interest in the creation of a range of devices including high-efficiency organic nanoscale light sources[7] and integrated nanoscale organic-lasers.

RESULTS AND DISCUSSION

The optical nanocavities that we have constructed are based on three missing air holes in a two-dimensional photonic crystal slab constructed into a SiN membrane of refractive index of $n = 2.1$. The free-standing membranes that we have used were purchased from Silson, Ltd. and consist of a 200 nm thick SiN layer having an area of ~0.25 mm^2 that is defined in a silicon wafer. Onto this free-standing membrane, a triangular 2DPC was written using electron beam lithography having a lattice constant of $a = 260$ nm with a diameter of 0.6*a*. A nanocavity was fabricated into the photonic crystal and consisted of three aligned missing air holes. To increase cavity *Q*-factor, the size of the four boundary air holes on the 'long-edge' above and below the cavity were reduced to 0.5*a*, with the size of the air holes at the ends of the cavity reduced to 0.4*a* and displaced away from the cavity center by a distance of $S = 0.22a$. This structure was then transferred into the SiN membrane using a CHF_3-based reactive ion etching technique. The final size of the photonic crystal was 146 μm^2. Figure 1a shows a schematic of the layout of the nanocavity, with parts b and c showing scanning electron microscopy (SEM) images of the nanocavity and surrounding photonic crystal taken at different magnifications.

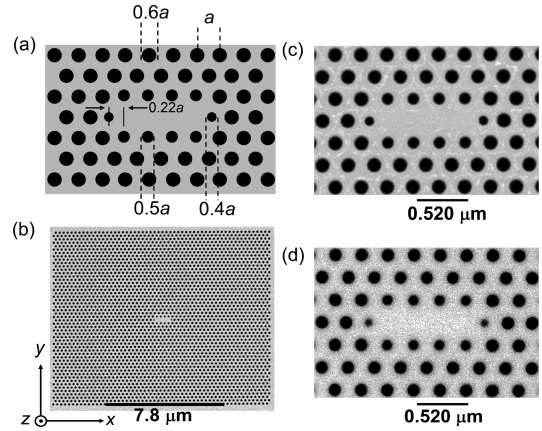

Figure 1. (a) A schematic diagram of the location and layout of the holes around the nanocavity explored in this work; (b, c) SEM images at two magnifications of the SiN-based photonic crystal nanocavity. Here, both images were recorded from the topmost surface of the structure. In part d we show an SEM image of the nanocavity recorded from the undersurface of a photonic crystal membrane.

In contrast to previous reports,[31,34−36] the holes defined in our structures are not exposed to a wet chemical-etch process that is usually used to remove a sacrificial layer beneath the structure to form an air-bridge. Such a wet-etch process is usually responsible for introducing an inadvertent taper in the side-walls of the holes in the photonic crystal. The low degree of taper present in the air holes can be evidenced using SEM. In Figure 1d, we show a SEM image of our structure taken from the underside of the free-standing membrane. It can be seen that the apparent size of the air-holes is reduced from 160 nm (membrane top surface) to 143 nm (membrane bottom surface), indicating that the taper of each side-wall is around 2.4°. This

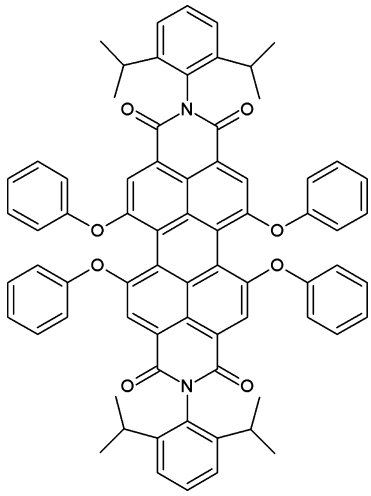

Figure 2. The chemical structure of Lumogen Red.

compares very favorably with previous work on SiN-based photonic crystal nanocavities, where a taper angle ranging from 4° to 8° was reported.[31]

To explore the effect of the cavity on a surface film of an organic semiconductor, we coated a 3 nm thick film of the molecular dye Lumogen Red onto the photonic crystal surface using thermal-evaporation. Lumogen Red (see chemical structure in Figure 2) has a high room-temperature photoluminescence quantum efficiency combined with high photostability even under extended exposure to sunlight.[22]

In Figure 3a, we plot the fluorescence emission spectrum of a control thin film of Lumogen Red (black line), along with the luminescence recorded from the nanocavity surface. As it can be seen, the luminescence emission recorded from the cavity is very similar in shape to that of the Lumogen Red control film, but onto which are superimposed a series of sharp peaks appearing at 668, 646, and 634.8 nm. We arbitrarily label these peaks as M1, M2, and M3, respectively. As these peaks are absent in the control Lumogen Red film, we conclude that these peaks result from the enhancement of the emission from the Lumogen Red as a result of a coupling between the molecular dipoles and the confined optical field in the underlying nanocavity. Note, that our previous work[32] has shown that the SiN itself is weakly luminescent and is enhanced by the nanocavity structure; however, such emission can only be detected following excitation using a laser whose intensity is at least 30 times more intense than that used here.

Further insight into the resonant modes observed in Figure 3a can be gained through measuring the emission from the cavity as a function of polarization angle. The results of these measurements are shown in Figure 3b. It can be seen that mode M1 is polarized along the *y*-axis (perpendicular to the cavity long axis) suggesting that it is the fundamental cavity-mode, while modes M2 and M3 are polarized along the *x*-axis (parallel to the cavity long axis). By fitting the emission

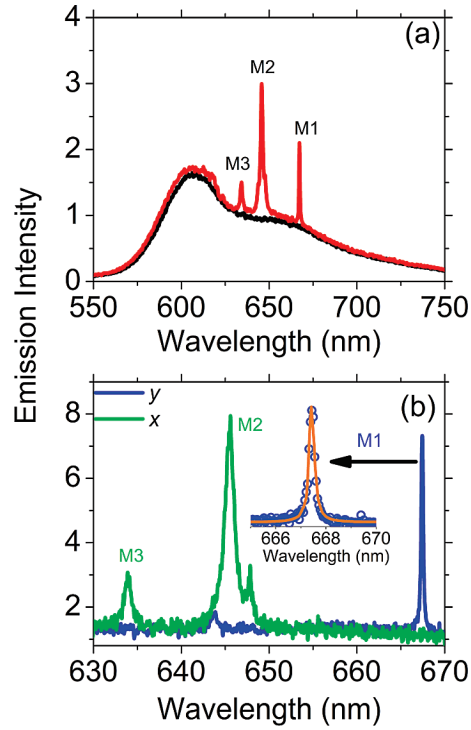

Figure 3. (a) Fluorescence emission of a control film of the molecular dye Lumogen Red (black line) together with the unpolarized fluorescence emission of the Lumogen Red when coated onto the nanocavity surface; (b) fluorescence emission of a Lumogen Red/SiN nanocavity recorded at a polarization perpendicular to (*y*-axis) and parallel to (*x*-axis) the cavity long axis. The inset shows an expanded portion of the emission spectra recorded perpendicular to the cavity axis centered around the wavelength corresponding to the M1 (fundamental cavity) mode. Here, the emission is fit to a Lorentzian function having a line width of 0.25 nm.

spectrum of mode M1 in Figure 3b using a Lorentzian function (see inset to Figure 3b) we deduce (using the full width half-maximum mode line width $\Delta\lambda$) that the cavity has a maximum cavity *Q*-factor (defined as $\lambda/\Delta\lambda$) of 2650. As far as we are aware, this *Q*-factor is the highest quality factor reported from a SiN-based 2DPC nanocavity containing a fluorescent organic dye.

To gain further insight into the experimental spectra presented in Figure 3, we have used three-dimensional finite difference time domain (FDTD) calculations[37] to simulate the optical properties of our structure. In the calculations we chose input parameters into the FDTD model to closely resemble the known structural parameters of the cavities that we have fabricated. In the calculations we set the photonic crystal size to be $34a \times 19\sqrt{3}a$ and the boundary conditions were implemented by introducing a perfect matching layer around the structure. In the calculations the emission was modeled in the form of a single dipole of polarization $\mathbf{P}(x,y,z) = (1,1,0)$ located at a weak symmetry point close the cavity surface.

Figure 4a shows a comparison between calculated and measured emission spectra. As it can be seen there is a very close similarity between the two spectra validating use of a single dipole to simulate the emission

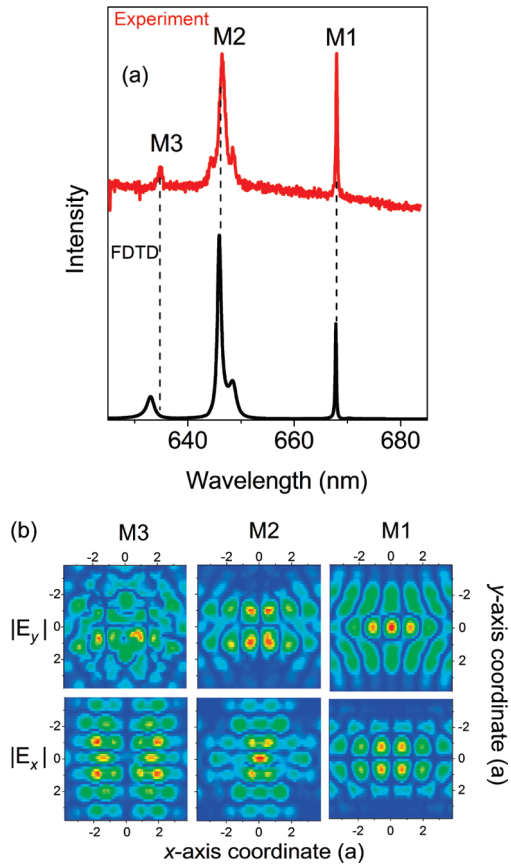

Figure 4. (a) Comparison between the measured unpolarized fluorescence emission spectrum from the Lumogen Red/SiN nanocavity (red line) and the simulated emission spectrum (black line) generated using our FDTD modeling; (b) predicted electromagnetic field at the cavity surface at wavelengths corresponding to modes M1, M2, and M3.

spectra of our structure. In particular, the FDTD emission spectrum contains three optical modes at 667.7, 645.8, and at 633 nm, with the mode at 667.7 nm being polarized along the *y*-axis. The calculations indicate that the two shorter wavelength modes are polarized along the *x*-axis in excellent agreement with experimental measurements. Furthermore, the FDTD calculations indicate that mode M1 has a *Q*-factor of 2900; a value in close agreement with the measured value of 2650. This close agreement suggests that optical loss resulting from both incoherent scattering and vertical asymmetry is strongly reduced in our cavity structures.

In Figure 4b, we plot the amplitude of the *x* and *y* components of the electromagnetic field calculated at the nanocavity surface for wavelengths corresponding to modes M1, M2, and M3. As it can be seen the fields associated with the optical modes are confined within the cavity region. The *y* component of the electric field distribution of the fundamental mode M1 has three antinodes within the cavity, with field maxima at the cavity center as expected for an *L*3 cavity.[27] In contrast, the *x* component of the electric field distribution of mode M1 has a field node at the cavity center. For mode M2, the *x* component of the field has an antinode at the cavity center, while the *y* component of the field has a node at the cavity center. As both modes M1 and M2 have a field antinode at the cavity center, it potentially makes them a very useful tool to modify the emission process of an emitting material that is located within the cavity or on the cavity surface. Mode M3 however has a field node at the cavity center for both *x* and *y* field components, and a field antinode close to the air holes that surround the cavity. This makes mode M3 less useful to study such effects as it potentially requires an emissive dipole to be positioned close to the air holes. Furthermore, the lack of clear symmetry of the *y* component of the optical field of mode M3 suggests that it is only weakly confined by the cavity.

Mode M1 is known to exhibit a small mode volume of $V = 1.32(\lambda/n)^3 = 0.042\ \mu m^3$,[31] yielding a Q/V figure of merit equal to 63 000 μm^{-3}. This makes our structures a suitable system to study the Purcell effect. Achieving a large increase in the overall spontaneous emission rate for an organic material using our cavity will however require a high spectral and spatial overlap between the emitting dipole of the organic material and the optical field of the cavity mode.[16,38] This will require a material having a narrow emission line width to be accurately deposited on the cavity surface at a region corresponding to the antinode of a confined optical field mode. Future work will address this using high precision lithographic patterning techniques such as near field optical lithography[39] or dip-pen lithography[40] to position a single emitter at the antinode of the M1 mode optical field. Such a technique will in principle permit us to explore the coupling of a single emitter to a confined field as has been demonstrated in self-assembled quantum dot based structures.[38,41]

CONCLUSIONS

We have fabricated organic nanocavities having a *Q*-factor of 2650. The ability to create such high *Q*-factor cavities results from the fact that our structures are directly fabricated on a free-standing SiN membrane, with the structures created not being subsequently exposed to a wet-etch stage. This technique allows us to create photonic crystals having a small (2.4°) air hole taper. We have used three-dimensional FDTD calculations to simulate the experimentally determined cavity emission spectra with a high degree of accuracy. The ability to create optical structures of increased finesse will have direct impact on the development of a range of organic-based photonic structures and devices.

EXPERIMENTAL SECTION

The optical properties of the nanocavities were investigated using far field optical spectroscopy. Excitation was provided in a dark field configuration by focusing the 442 nm line of a HeCd laser onto a 2500 μm^2 spot on the sample surface, with the laser delivered to the surface at an angle of 45° relative to the sur-

face normal. We estimate that the excitation power density at the sample surface was ~15 W cm^{-2}. The photoluminescence emission from the cavities was collected at normal incidence from the sample surface using a 50× objective lens with a numerical aperture of 0.42 and was then directed toward a 0.25 m spectrometer where it was dispersed onto a nitrogen cooled CCD having a spectral resolution of 0.7 Å. To limit the emission recorded to that generated from the nanocavity alone (and not the surrounding photonic crystal), all emission spectra were recorded with the spectrometer slit width reduced to 0.01 mm with the emission collected from the rows on the CCD corresponding to the cavity image.

Acknowledgment. This work was supported by the UK EPSRC through Grant EP/D064767/1 "Nanoscale organic photonic structures". M. Murshidy thanks the Egyptian Ministry of Education for the award of a Ph.D. studentship. We also thank A. Boehm and Colorflex GmbH for the gift of the Lumogen Red used in these experiments.

REFERENCES AND NOTES

1. Haugeneder, A.; Neges, M.; Kallinger, C.; Spirkl, W.; Lemmer, U.; Feldmann, J. Exciton Diffusion and Dissociation in Conjugated Polymer/Fullerene Blends and Heterostructures. *Phys. Rev. B* **1999**, *59*, 15-346–15-351.
2. Alvarado, S. F.; Seidler, P. F.; Lidzey, D. G.; Bradley, D. D. C. Direct Determination of the Exciton Binding Energy of Conjugated Polymers Using a Scanning Tunneling Microscope. *Phys. Rev. Lett.* **1998**, *81*, 1082–1085.
3. Vanden Bout, D. A.; Yip, W.-T.; Hu, D.; Fu, D.-K.; Swager, T. M.; Barbara, P. F. Discrete Intensity Jumps and Intramolecular Electronic Energy Transfer in the Spectroscopy of Single Conjugated Polymer Molecules. *Science* **1997**, *277*, 1074–1077.
4. Xiong, Z. H.; Wu, D.; Vardeny, Z. V.; Shi, J. Giant Magnetoresistance in Organic Spin-Valves. *Nature* **2004**, *427*, 821–824.
5. Kirova, N. Understanding Excitons in Optically Active Polymers. *Polym. Int.* **2008**, *57*, 678–688.
6. Burroughes, J. H.; Bradley, D. D. C.; Brown, A. R.; Marks, R. N.; Mackay, K.; Friend, R. H.; Burn, P. L.; Holmes, A. B. Light-Emitting Diodes Based on Conjugated Polymers. *Nature* **1990**, *347*, 539–541.
7. Boroumand, F. A.; Fry, P. W.; Lidzey, D. G. Nanoscale Conjugated-Polymer Light-Emitting Diodes. *Nano Lett.* **2005**, *5*, 67–71.
8. Kuwata-Gonokami, M.; Takeda, K. Polymer Whispering Gallery Mode Lasers. *Opt. Mater.* **1998**, *9*, 12–17.
9. Bulovic, V.; Kozlov, V. G.; Khalfin, V. B.; Forrest, S. R. Transform-Limited, Narrow-Linewidth Lasing Action in Organic Semiconductor Microcavities. *Science* **1998**, *279*, 553–555.
10. Yap, B. K.; Xia, R.; Campoy-Quiles, M.; Stavrinou, P. N.; Bradley, D. D. C. Simultaneous Optimization of Charge-Carrier Mobility and Optical Gain in Semiconducting Polymer Films. *Nat. Mater.* **2008**, *7*, 376–380.
11. Samuel, I. D. W.; Turnbull, G. A. Organic Semiconductor Lasers. *Chem. Rev.* **2007**, *107*, 1272–1295.
12. Frolov, S. V.; Shkunov, M.; Vardeny, Z. V.; Yoshino, K. Ring Microlasers from Conducting Polymers. *Phys. Rev. B* **1997**, *56*, R4363–R4366.
13. Sudzius, M.; Langner, M.; Hintschich, S. I.; Lyssenko, V. G.; Fröb, H.; Leo, K. Multimode Laser Emission from Laterally Confined Organic Microcavities. *Appl. Phys. Lett.* **2009**, *94*, 061102.
14. Koschorreck, M.; Gehlhaar, R.; Lyssenko, V. G.; Swoboda, M.; Hoffmann, M.; Leo, K. Dynamics of a High-*Q* Vertical-Cavity Organic Laser. *Appl. Phys. Lett.* **2005**, *87*, 181108.
15. Purcell, E. M. Spontaneous Emission Probabilities at Radio Frequencies. *Phys. Rev.* **1946**, *69*, 681.
16. Gérard, J. M.; Gayral, B. Strong Purcell Effect for InAs Quantum Boxes in Three-Dimensional Solid-State Microcavities. *J. Lightwave Technol.* **1999**, *17*, 2089–2095.
17. Strauf, S.; Hennessy, K.; Rakher, M. T.; Choi, Y. S.; Badolato, A.; Andreani, L. C.; Hu, E. L.; Petroff, P. M.; Bouwmeester, D. Self-Tuned Quantum Dot Gain in Photonic Crystal Lasers. *Phys. Rev. Lett.* **2006**, *96*, 127104.
18. Strangi, G.; Barna, V.; Caputo, R.; Luca, A. D.; Versace, C.; Scaramuzza, N.; Umeton, C.; Bartolino, R. Color-Tunable Organic Microcavity Laser Array Using Distributed Feedback. *Phys. Rev. Lett.* **2005**, *94*, 063903.
19. Lidzey, D. G.; Bradley, D. D. C.; Skolnick, M. S.; Virgili, T.; Walker, S.; Whittaker, D. M. Strong Exciton−Photon Coupling in an Organic Semiconductor Microcavity. *Nature* **1998**, *395*, 53–55.
20. Connolly, L. G.; Lidzey, D. G.; Butte', R.; Adawi, A. M.; Whittaker, D. M.; Skolnick, M. S.; Airey, R. Strong Coupling in High-Finesse Organic Semiconductor Microcavities. *Appl. Phys. Lett.* **2003**, *83*, 5377–5379.
21. Kèna-Cohen, S.; Davanco, M.; Forrest, S. R. Strong Exciton-Photon Coupling in an Organic Single Crystal Microcavity. *Phys. Rev. Lett.* **2008**, *101*, 116401.
22. Adawi, A. M.; Cadby, A.; Connolly, L. G.; Hung, W. C.; Dean, R.; Tahraoui, A.; Fox, A. M.; Cullis, A. G.; Sanvitto, D.; Skolnick, M. S.; Lidzey, D. G. Spontaneous Emission Control in Micropillar Cavities Containing a Fluorescent Molecular Dye. *Adv. Mater.* **2006**, *18*, 742–747.
23. Langner, M.; Gehlhaar, R.; Schriever, C.; Fröb, H.; Lyssenko, V. G.; Leo, K. Strong Optical Confinement and Multimode Emission of Organic Photonic Dots. *Appl. Phys. Lett.* **2007**, *91*, 181119.
24. Buck, J. R.; Kimble, H. J. Optimal Sizes of Dielectric Microspheres for Cavity QED with Strong Coupling. *Phys. Rev. A* **2003**, *67*, 033806.
25. Joannopoulos, J. D.; Johnson, S. G.; Win, J. N.; Meade, R. D. *Photonic Crystals: Modelling the Flow of Light* 2nd ed.; Princeton University: Princeton, New Jersey, 1995; pp 66−92 and pp 135−155.
26. Joannopoulos, J. D.; Villeneuve, P. R.; Fan, S. Photonic Crystals: Putting a New Twist on Light. *Nature* **1997**, *386*, 143–149.
27. Akahane, Y.; Asano, T.; Song, B. S.; Noda, S. High-*Q* Photonic Nanocavity in a Two-Dimensional Photonic Crystal. *Nature* **2003**, *425*, 944–947.
28. Adawi, A. M.; Chalcraft, A. R. A.; Whittaker, D. M.; Lidzey, D. G. Refractive Index Dependence of *L*3 Photonic Crystal Nanocavities. *Opt. Express* **2007**, *15*, 14299–14305.
29. Noda, S. Recent Progresses and Future Prospects of Two- and Three-Dimensional Photonic Crystals. *J. Lightwave Technol.* **2006**, *24*, 4554–4567.
30. Kitamura, M.; Iwamoto, S.; Arakawa, Y. Enhanced Light Emission from an Organic Photonic Crystal with a Nanocavity. *Appl. Phys. Lett.* **2005**, *87*, 151119.
31. Barth, M.; Kouba, J.; Stingl, J.; Löchel, B.; Benson, O. Modification of Visible Spontaneous Emission with Silicon Nitride Photonic Crystal Nanocavities. *Opt. Express* **2007**, *15*, 17231–17240.
32. Murshidy, M. M.; Adawi, A. M.; Fry, P. W.; Whittaker, D. M.; Lidzey, D. G. The Optical Properties of Hybrid Organic−Inorganic *L*3 Nanocavities. *J. Opt. Soc. Am. B* **2010**, *27*, 215–221.
33. Tanaka, Y.; Asano, T.; Akahane, Y.; Song, B.-S.; Noda, S. Theoretical Investigation of a Two-Dimensional Photonic Crystal Slab with Truncated Cone Air Holes. *Appl. Phys. Lett.* **2003**, *82*, 1661–1663.
34. Park, H. G.; Barrelet, C. J.; Wu, Y.; Tian, B.; Qian, F.; Lieber, C. M. A. Wavelength-Selective Photonic-Crystal Waveguide Coupled to a Nanowire Light Source. *Nat. Photonics* **2008**, *2*, 622–626.
35. Neal, R. T.; Zoorob, M. E.; Charlton, M. D.; Parker, G. J.; Finlayson, C. E.; Baumberg, J. J. Photonic Bandgaps in Patterned Waveguides of Silicon-Rich Silicon Dioxide. *Appl. Phys. Lett.* **2004**, *84*, 2415–2417.
36. Netti, M. C.; Charlton, M. D. B.; Parker, G. J.; Baumberg, J. J. Visible Photonic Band Gap Engineering in Silicon Nitride Waveguides. *Appl. Phys. Lett.* **2000**, *76*, 991–993.
37. The 3D FDTD code (CrystalWave) used in this work is a product of Photon Design Ltd, http://www.photond.com.
38. Englund, D.; Fattal, D.; Waks, E.; Solomon, G.; Zhang, B.; Nakaoka, T.; Arakawa, Y.; Yamamoto, Y.; Vučković, J.

Controlling the Spontaneous Emission Rate of Single Quantum Dots in a Two-Dimensional Photonic Crystal. *Phys. Rev. Lett.* **2005**, *95*, 013904.
39. Sung, S.; Leggett, G. L. Matching the Resolution of Electron Beam Lithography by Scanning Near-Field Photolithography. *Nano Lett.* **2004**, *4*, 1381–1384.
40. Haaheim, J.; Eby, R.; Nelson, M.; Fargala, J.; Rosner, B.; Zhang, H.; Athas, G. Dip Pen Nanolithography (DPN): Process and Instrument Performance with NanoInk's Scriptor System. *Ultramicroscopy* **2005**, *103*, 117–132.
41. Nomura, M.; Kumagai, N.; Iwamoto, S.; Ota, Y.; Arakawa, Y. Laser Oscillation in a Strongly Coupled Single-Quantum-Dot-Nanocavity System. *Nat. Phys.* **2010**, *6*, 279–283.